JOURNAL OF GEOPHYSICAL RESEARCH, VOL. ???, XXXX, DOI:10.1029/,

Spectroscopic diagnostics of laboratory air plasmas as a benchmark for spectral rotational (gas) temperature determination in TLEs

F. C. Parra-Rojas[1], M. Passas[1], E. Carrasco[2, 4], A. Luque[1], I. Tanarro[2], M. Simek[3]

and F. J. Gordillo-Vázquez[1]

Abstract. We have studied laboratory low pressure (0.1 mbar ≤ p ≤ 2 mbar) glow air discharges by optical emission spectroscopy to discuss several spectroscopic techniques that could be implemented by field spectrographs, depending on the available spectral resolution, to experimentally quantify the gas temperature associated to TLEs occurring at different altitudes including blue jets,

F. C. Parra-Rojas, Instituto de Astrofísica de Andalucía (IAA), CSIC, PO Box 3004, 18080 Granada, Spain. (fpr@iaa.es)

M. Passas, Instituto de Astrofísica de Andalucía (IAA), CSIC, PO Box 3004, 18080 Granada, Spain. (passasv@iaa.es)

E. Carrasco, Instituto de Estructura de la Materia (IEM), CSIC, Serrano 123, 28006 Madrid, Spain. (esther.carrasco@fau.de). Present address: Chair of Physical-Chemistry II, Erlangen-Nuremberg University, Egerlandstr. 3, D-91058, Erlangen, Germany.

A. Luque, Instituto de Astrofísica de Andalucía (IAA), CSIC, PO Box 3004, 18080 Granada, Spain. (aluque@iaa.es)

I. Tanarro, Instituto de Estructura de la Materia (IEM), CSIC, Serrano 123, 28006 Madrid, Spain. (itanarro@iem.cfmac.csic.es)

M. Simek, Department of Pulse Plasma Systems, Institute of Plasma Physics v.v.i., Academy of Sciences of the Czech Republic, Za Slovankou 3, 182 00 Prague, Czech Republic. (simek@ipp.cas.cz)

F. J. Gordillo-Vázquez, Instituto de Astrofísica de Andalucía (IAA), CSIC, PO Box 3004, 18080 Granada, Spain. (vazquez@iaa.es)

[1]Instituto de Astrofísica de Andalucía (IAA),

giant blue jets and sprites. Laboratory air plasmas have been analysed from the near UV (300 nm) to the near IR (1060 nm) with high (up to 0.01 nm) and low (2 nm) spectral resolution commercial grating spectrographs and by an inhouse intensified CCD grating spectrograph that we have recently developed for TLE spectral diagnostic surveys with $\simeq$ 0.45 nm spectral resolution. We discuss the results of lab tests and comment on the convenience of using one or another technique for rotational (gas) temperature determination depending on the altitude and available spectral resolution. Moreover, we compare available low resolution (3 nm $\leq \Delta\lambda \leq$ 7 nm) N_2 1PG field recorded sprite spectra at 53 km ($\simeq$ 1 mbar), and resulting vibrational distribution function (VDF), with 1 mbar lab-

CSIC, PO Box 3004, 18080 Granada, Spain

[2]Instituto de Estructura de la Materia (IEM),
CSIC, Serrano 123, 28006 Madrid, Spain

[3]Department of Pulse Plasma Systems,
Institute of Plasma Physics v.v.i., Academy of
Sciences of the Czech Republic, Za Slovankou
3, 182 00 Prague, Czech Republic

[4]Present address: Chair of
Physical-Chemistry II, Erlangen-Nuremberg
University, Egerlandstr. 3, D-91058, Erlangen,
Germany.

oratory glow discharge spectrum ($\Delta\lambda$ = 2 nm) and synthetic sprite spectra from models. We found that while the relative population of $N_2(B^3\Pi_g, v = 2-7)$ in sprites and laboratory produced air glow plasmas are similar, the $N_2(B^3\Pi_g, v = 1)$ vibrational level in sprites is more efficiently populated (in agreement with model predictions) than in laboratory air glow plasmas at similar pressures.

1. Introduction

The ocurrence of different types of transient luminous events (TLEs) in the Earth's atmosphere can contribute to the heating of the surrounding air. In particular, air heating is possible in different layers of the atmosphere in streamers of sprites [*Pasko et al.*, 1998], giant blue jets and blue jets [*Wescott et al.*, 2001] as well as in the streamer to leader transition in the bottom of blue jets and giant blue jets [*Riousset et al.*, 2009, 2010]. Therefore, the chemistry and electrical properties of the atmosphere can be influenced by these "hot spot" regions associated to TLE activity with higher (than background) gas temperature. Since the first TLE image reported by *Franz et al.* [1990], several observational campaings have clarified the nature of the different TLE optical emissions. Spectroscopic studies of TLEs started in the mid 1990s, when the simultaneous works by *Mende et al.* [1995] and *Hampton et al.* [1996] provided the first spectroscopic studies of the red N_2 1PG sprite optical emissions at standard video rate in the 550 nm - 840 nm spectral range at low (between 10 nm and 6 nm) spectral resolutions. In a paper published in 2001, *Wescott et al.* [2001] used a narrowband (1.25 nm) filter to measure the N_2^+ 1NG (0,1) band emission at 427.8 nm, which provided the first direct evidence for the ionization of blue starters and blue jets reaching a maximum altitude of about 40 km. In 2002, *Morrill et al.* [2002] also reported aircraft observations of the N_2^+ 1NG (0,1) band at 427.8 nm and N_2 2PG (0,0) band at 337.0 nm from sprites. The 1NG/2PG intensity ratios measured by *Morrill et al.* [2002] showed two distinct regions, above and below 55 km. They suggested a relative enhancement of ion emission below 55 km (region of sprite "tendrils") based on high speed (1000 fps) video recordings by *Moudry et al.* [2002] showing that while sprite "tendril" emissions last for $\sim$ 1 ms, sprite "body" emissions occur during a longer time gap of $\sim$ 10 ms

and, as reported by *Morrill et al.* [2002], these time scales are consistent with ionization taking place during short times (~ 1 ms) at 40 - 55 km [*Armstrong et al.*, 1998; *Suszcynsky et al.*, 1998; *Armstrong et al.*, 2000] and with longer neutral emissions dominating above 55 km [*Morrill et al.*, 2002]. So, depending on the altitude, the species responsible for the TLE optical emissions change from being mostly excited neutrals ($N_2(B^3\Pi_g)$ and $N_2(C^3\Pi_u)$) for higher altitudes (55 km up to 85 km) to a balance at lower heights (55 km and below) between the emissions from excited neutrals (mainly $N_2(C^3\Pi_u)$) and excited ions ($N_2^+(B^2\Sigma_u^+)$).

The rotational temperature derived from the optical emissions produced by an excited electronic state of a diatomic molecule is a correct measurement of the gas temperature only if the rotational distribution of a given electronically excited state is thermalized, that is, if it follows a Boltzmann distribution of rotational levels of the ground electronic state. The latter occurs when the characteristic rotation-translation relaxation time is much smaller than the characteristic time of the primary deexcitation process (the radiative lifetime at sufficiently low pressure or the collisional quenching time at higher pressures [*Lavrov et al.*, 2003]). The radiative lifetime of the highest vibrational level ($v = 12$) of $N_2(B^3\Pi_g)$ is around 4 μs and the corresponding values of $v = 3$, 2, 1, and 0 of $N_2(B^3\Pi_g)$ are, respectively, about 7.3, 8.5, 9.7 and 12.1 μs. On the other hand, the radiative lifetimes of $N_2^+(B^2\Sigma_u^+)$ and $N_2(C^3\Pi_u)$ are 60 ns and 40 ns, respectively. Assuming that 2 - 3 collisions are usually enough to thermalize the rotational distributions of $N_2(B^3\Pi_g)$, $N_2(C^3\Pi_u)$ and $N_2^+(B^2\Sigma_u^+)$, we can determine the pressure dependent characteristic rotation-translation relaxation time of N_2 [*Biloiu et al.*, 2007]. Therefore, due to these differences in radiative lifetimes, the low pressure (high altitude) limit for achieving thermalization (assuming $T_{gas} = 220$ K) of the rotational manifold of the $N_2(B^3\Pi_g)$ changes with vibrational level. The highest altitude limit is in fact associated only with the $v' = 0$, and for the (0, v'')

bands of the $N_2(B^3\Pi_g \rightarrow A^3\Sigma_u^+)$ transition (N_2 1PG) it has a value around $\simeq$ 75 km (0.03 mbar), whereas the highest altitude limit is $\simeq$ 68 km (0.08 mbar) for the (12, v'') bands of the N_2 1PG, it is 60 km (0.70 mbar) for $N_2^+(B^2\Sigma_u^+)$ and is 50 km (1 mbar) for $N_2(C^3\Pi_u)$. On the other hand, quenching rate coefficients of $N_2(B^3\Pi_g)$ by N_2 are (1-8) $\times 10^{-11}$ cm^3 s^{-1} for v = 0 - 12 [*Piper*, 1988]. Then, for the 0.03 mbar lowest pressure limit ($\simeq$ 75 km altitude), the characteristic time of the quenching process, which is the other channel that competes **with** the deactivation of the $N_2(B^3\Pi_g)$ state, is roughly one order of magnitude longer than rotational-translational relaxation time. As we decrease in altitude, collisional (quenching) deactivation tends to dominate over radiative decay of $N_2(B^3\Pi_g)$, $N_2^+(B^2\Sigma_u^+)$ and $N_2(C^3\Pi_u)$. The quenching heights (h_q) indicate the altitudes above which quenching is negligible, while below h_q collisional deactivation effects begin to be severe. The h_q for $N_2(B^3\Pi_g)$, $N_2^+(B^2\Sigma_u^+)$ and $N_2(C^3\Pi_u)$ are around 53 km, 48 km and 30 km, respectively [*Vallance Jones*, 1974]. For sufficiently high pressures (when quenching dominates), the rotational temperatures derived from surviving $N_2(B^3\Pi_g)$, $N_2^+(B^2\Sigma_u^+)$ or $N_2(C^3\Pi_u)$ optical emissions from some TLEs (like blue jets and/or giant blue jets) below h_q can only be considered reliable if collisional quenching times (τ_q) remain longer that rotational-translational relaxation times. The previous considerations can be useful as an indication of the emitting species in TLEs that could be tracked to determine the rotational (gas) temperature by spectroscopic means at different altitudes.

The scientific goals of this work are mainly three. (a) To **test** hollow cathode (HC) air discharges as laboratory analog discharges of TLEs; (b) to test and compare three different spectroscopic techniques to quantify the rotational (gas) temperature in air discharges with the aim to use them in TLE spectral diagnosis and, (c) to test the capabilities of a recently inhouse **developed** field instrument called GRAnada Sprite Spectrograph and Polarimeter (GRASSP),

with a nominal spectral resolution of 0.45 nm, that we will use for TLE spectroscopic surveys in Europe.

In this work, we use three different methods of gas temperature determination that **employ** (a) the rotational R - branch (ΔJ = +1) of the vibrational transition (0,0) of the first negative system of $N_2^+(B^2\Sigma_u^+ \rightarrow X^2\Sigma_g^+)$ when the resolution of the spectrograph is high enough (0.005 nm - 0.05 nm) to resolve the rotational structure (this is the so called Boltzmann plot method [*Herzberg*, 1950]), (b) a method proposed by *Simek and DeBenedictis* [1995] based on the analysis of several peaks appearing in low lying vibrational transitions, specifically (3,0), (2,0), (1,0) and (0,0), of the first positive group of $N_2(B^3\Pi_g \rightarrow A^3\Sigma_u^+)$, or $N_2(B^3\Pi_g)$ 1PG, that can be used when medium (0.1 nm - 0.5 nm) resolution spectrographs are available, and (c) a method based on the numerical fitting of synthetic spectrum to the observed (measured) spectrum of the envelope of selected (v', v'') bands of the $N_2(B^3\Pi_g)$ 1PG recorded with medium (0.1 nm - 0.5 nm) resolution spectrographs. The spectra recorded in the laboratory will also be used as a test for the GRAnada Sprite Spectrograph and Polarimeter (GRASSP) instrument recently developed at our institute in order to start spectroscopic field campaigns of TLEs in Spain as ground support to the Atmosphere Space Interaction Monitor (ASIM) mission of ESA and to the TARANIS mission of CNES, both to be launched in late 2015. In this sense, the spectra (corrected by instrument spectral response) of a 0.2 mbar air commercial discharge lamp taken by GRASSP will be compared with the spectra of air discharges produced at similar (0.23 mbar) pressure within DC hollow cathode reactors recorded by laboratory commercial spectrographs. After the gas temperature is obtained, we will be able to extract the vibrational distribution function (VDF) of $N_2(B^3\Pi_g)$ by fitting a synthetic spectrum of the $N_2(B^3\Pi_g)$ 1PG to the recorded/observed spectrum at low resolution (2 nm). The latter will be used to obtain partial ($1 \leq v \leq 7$) VDFs of

$N_2(B^3\Pi_g)$ in air plasmas produced in laboratory DC hollow cathode discharges (0.1 mbar - 2 mbar) that will be compared with the experimental $N_2(B^3\Pi_g)$ VDF in sprites derived by *Bucsela et al.* [2003] at 53 km ($\simeq$ 1 mbar) and *Kanmae et al.* [2007] at 53 km and with theoretical predictions of $N_2(B^3\Pi_g)$ VDF in halos and sprites [*Gordillo-Vázquez*, 2008], [*Gordillo-Vázquez*, 2010; *Luque and Gordillo-Vázquez*, 2011; *Gordillo-Vázquez et al.*, 2011, 2012]. Previous experimental and modeling works on the kinetics and vibrational level populations of N_2 triplet states were done to investigate N_2 emissions in low altitude auroras [*Cartwright*, 1978; *Morrill and Benesch*, 1996] and N_2 afterglow discharges [*Piper*, 1988, 1989].

In the following we will first comment in section 2 on the experimental details of this work, then we will describe in section 3 the spectroscopic methods used to determine the rotational (gas) temperature whose results will be discussed in section 4. The paper is finished with a summary and conclusions in section 5 where we also provide recommendations of the spectroscopic methods and conditions that we believe are the best for remote quantification of the rotational (gas) temperature in TLE produced air plasmas in the earth atmosphere.

2. Experimental details

2.1. Experimental set-up for hollow cathode discharges in air

Non-thermal low temperature plasmas of air were produced by means of a low pressure, hollow cathode discharge reactor, which was used previously to study plasmas of air [*Castillo et al.*, 2004b] and nitrogen oxides [*de los Arcos et al.*, 1998; *Castillo et al.*, 2002, 2004a]. Hollow cathode discharges provide a uniform, stable, and relatively intense light emission in the negative glow, as well as gas temperatures close to the room ones, which render clear advantages for spectroscopic purposes related with atmospheric research. The detailed description of the reactor is given elsewhere [*Castillo et al.*, 2004b; *de los Arcos et al.*, 1998]. It has a modular

configuration, suitable for emission [*Castillo et al.*, 2004b] and absorption spectroscopy [*de los Arcos et al.*, 1998], as well as for mass spectrometry and the use of electrical probes [*Castillo et al.*, 2004b; *de los Arcos et al.*, 1998], with the proper selection of the different adaptors or windows to be employed at its two ends. We can see in Figure 1 the experimental set up of the hollow cathode discharge used and an image of the air plasma produced. In brief, it has cylindrical electrode geometry and consists of a grounded stainless steel hollow cathode, 16 mm inner diameter, 90 mm long, and two circular copper anodes, placed symmetrically at the ends of the cathode to ensure the uniformity and extension of the negative glow along the whole cathode length. The total volume of the cell is 130 cm^3. The electrodes are refrigerated by circulating water. The discharge is fed by a DC source, able to supply up to 2 kV and 200 mA. Plasma currents $\simeq$ 20 - 100 mA and voltages $\simeq$ 350 - 450 V were applied during the present experiments. The discharge was sustained in a continuous flow of natural air ($\simeq$ 5 - 20 sccm), at pressures of 0.1 - 2 mbar. Pressure and gas flow were regulated by a needle valve at the input, and a rotary pump with a regulating valve at the exit.

Diffusion of excited species to the cathode walls, where they might collide and experiment de-excitation, is described by Fick′s Law [*Levine*, 1978; *McDaniel*, 1989]. We have assumed a model of rigid spheres and employed the effective diameters of N_2 and O_2 from *Hirschfelder* [1954] to estimate the typical diffusion times along the cathode radius, as it was done in *Castillo et al.* [2004a, b] and *de los Arcos et al.* [1998]. Under the present air pressures ranging from 0.1 to 2 mbar these diffusion times result to be within the interval 0.1 - 1 ms, considerably longer than the radiative lifetimes of the excited N_2 and N_2^+ levels in this work, whereas the average time between successive collisions at these pressures (equivalent to some 68 - 50 altitudes) are of some 10^{-6} - 10^{-7} s, respectively [*McDaniel*, 1989].

Complete emission spectra of the plasmas were recorded in the 300 - 1060 nm wavelength range through a BK7 optical window. A red filter (cut off at 600 nm) was used to avoid second order lines in spectra taken at wavelengths above this value. The light from the discharge was transmitted by an optical fibre imaged on the entrance slit of a Jobin Yvon-HORIBA FHR1000 spectrometer, 1 m focal length, in Czerny-Turner configuration, with two concave mirrors and two interchangeable planar gratings of 1200 and 1800 grooves/mm, and was detected by a front exit SYNAPSE^{TM} CCD camera, or a side exit photomultiplier Hamamatsu R928P. The spectral resolution of the FHR1000 spectrometer spans from 0.006 nm to 0.13 nm, depending on the slit widths, grating and detector used. This resolution can be numerically lowered by convolution of the acquired spectra with a Gaussian profile of the desired width to simulate broader line profiles. With this method, one can apply easily some of the analytical procedures for gas temperature estimations proposed here (see below), or can compare the originally high resolution spectra with the spectra obtained with lower resolution field spectrometers. Alternatively, an Ocean QE65000 spectrograph with 300 grooves/mm grating, 25 μm slit width and CCD was employed, supplying 2 nm spectral resolution spectra. The spectral efficiency calibrations of these instruments were obtained from their spectral responses to the emission of a previously calibrated 500 W tungsten lamp. The spectra acquisition times were selected, depending on the spectrometer, detector and spectral resolution used in each case, in order to obtain signal to noise ratios in the spectra of the HC discharges good enough for not being a limiting factor in the temperature estimation methods proposed here. These signal to noise ratios increased even more with the convolution process employed to decrease the spectral resolution of the spectra originally taken with the FHR1000. It should be mentioned that the improvement of signal

to noise ratios is of vital interest in measurements of very short emission features like those produced by TLEs

2.2. Brief description of GRASSP

The instrument GRASSP (GRanada Sprite Spectrograph and Polarimeter) is formed by a spectrograph and a polarimeter, being each of them located in the two arms of a mobile mount. So far, only the spectrograph is used and it consists of a f/3.4 and 170 mm focal length lens telescope which can gather an optical beam at its focal plane, where an entrance slit of about 100 μm is placed before a F/3.8 and 190 mm focal length field lens, in order to define the observed field of view of 4 degrees and prevent vignetting. The slit is oriented parallel to the horizon to optimize the likelihood of TLE detection. After the field lens, a F/2.8 and 135 mm focal length collimator is placed to narrow the beam that will reach the dispersive element. After the 1440 grooves/mm and 70×70 mm aperture diffraction grating, a commercial intensified (60 dB + 30 dB) CCD camera of 1360 x 1024 pixels, 0.01 mm/px, F/1.7 and 50 mm in focal length provides the spectral pattern on the detector. The described spectrograph provides a free spectral range of 110 nm (650 nm to 760 nm), with a mean spectral resolution of R = $\lambda/\Delta\lambda$ = 1500; $\Delta\lambda$ = 0.45 nm. A calibrated halogen tungsten spectral lamp was used in order to obtain the spectroscopic system response and to make further spectral efficiency corrections. In order to test it, the spectra of three different commercial cylindrical lamps of N_2, air and Ne at 0.2 mbar, with the electrodes separated by a distance of 26 cm (0.5 cm width) fed by a 5 kV, 10 mA DC source, were used. The spectra obtained from these commercial lamps were corrected by the instrument spectral sensitivity response function and compared to the spectra of air plasmas produced in DC hollow cathode reactors under similar gas pressure (0.23 mbar) to check the instrument performance.

3. Spectroscopic methods

In this section we will describe the three spectroscopic methods used, together with their range of applicabiliby, to determine the rotational (gas) temperature of laboratory air plasmas produced at pressures (0.1 mbar (≃ 70 km) ≤ p ≤ 2 mbar (≃ 45 km)), similar to the ones under which TLE air plasmas are produced in the earth atmosphere.

3.1. Gas temperature by spectral analysis of low pressure air and N_2 plasmas

3.1.1. Rotational structure of $N_2^+(B^2\Sigma_u^+, v' = 0 \rightarrow X^2\Sigma_g^+, v'' = 0)$

When the resolution of the spectrograph employed is high enough (between 0.005 nm and 0.05 nm), we can use different bands of the first negative system of N_2^+, that is N_2^+ -1NG, to determine the rotational (gas) temperature by optical emission spectroscopy. In order to use this method, we first need to choose a particular (v', v'') band and determine the conditions under which the emitting rotational levels are in thermal (Boltzmann) equilibrium. Then, the intensity of the emission lines in a rovibronic band, being J' and J'' the rotational quantum numbers of the upper and lower rotational levels, is given by the thermal distribution of the emitting rotational levels as

$$I_{em}(T_R) = \frac{C_{em} \times \nu^4}{Q_R} \times (J' + J'' + 1) \times e^{-B_{v'} J'(J'+1)hc/kT_R}, \quad (1)$$

where T_R is the rotational temperature, C_{em} is a constant depending on the change of the dipole moment and the total number of molecules in the initial vibrational level (v') [*Herzberg*, 1950] and ν, Q_R and $B_{v'}$ are, respectively, the frequency, the rotational partition function and the first order rotational constant of the upper vibrational level (v') of the excited state $N_2^+(B^2\Sigma_u^+)$. The symbols c, h and k stand for the speed of light and the Planck and Boltzmann constants, respectively. Since the second order rotational constant $D_{v'}$ is usually $10^{-5}B_{v'}$, equation (1)

remains a good approximation for low $J' \leq 25$ (as in our case). From equation (1) we have

$$\ln F = A - \frac{B_{v'} J'(J'+1)hc}{kT_R} \tag{2}$$

where F = $I_{em}/(J'+J''+1)$ and A = $\ln(C_{em}\nu^4/Q_R)$ is almost constant for a given rotation-vibration band at a given temperature. We can see from equation (2) that by plotting $\ln(I_{em}/(J'+J''+1))$ against $J'(J'+1)$ a straight line is obtained whose slope is $B_{v'}hc/kT_R$. Thus, if the relative line emission intensities (I_{em}) have been measured and the rotational constant $B_{v'}$ of the excited state $N_2{}^+(B^2\Sigma_u^+)$ is known, the rotational temperature (T_R) of the emitting source can be obtained [*Herzberg*, 1950]. This way of obtaining T_R remains valid as long as the excitation of the emitting levels is purely thermal or if they are excited in electron-impact collisions. If other excitation channels (such as collisions with other neutrals, dissociation of molecules and/or recombination of molecular ions in electric discharges) come into play, the population distribution of the emitting levels can considerably deviate from the thermal (Boltzmann) distribution. We see in Figure 2 an example of a Boltzmann plot corresponding to the case of 1.5 mbar ($\simeq$ 48 km) obtained with the hollow cathode discharge and the Jobin-Yvon spectrometer with the CCD and the 1800 grooves/mm grating, using a spectral resolution of 0.023 nm. The two lines correspond to the fits of the even (blue line) and odd (red line) J'' values resulting in gas temperatures of 474 K and 426 K, respectively. The difference in temperatures is within 10 % discrepancy, attributable to the experimental uncertainty in line intensity measurements. The rotational (gas) temperature that we consider is the mean value (450 K) of the even and odd J'' fits.

3.1.2. Subband head peaks of $N_2(B^3\Pi_g, v' \rightarrow A^3\Sigma_u^+, v'')$ vibrational transitions

Given a certain (v', v'') band of the first positive group of N_2 , that is, $N_2(B^3\Pi_g \rightarrow A^3\Sigma_u^+)$ (or simply N_2 - 1PG), *Simek and DeBenedictis* [1995] proposed a method to estimate the gas temperature. It is based on the use of the ratios of the intensities of three selected peaks (I_1, I_2

and I_3) formed by the three sub-band heads of the (3,0) transition. The upper $N_2(B^3\Pi_g)$ state, with spin and orbital quantum numbers $S = 1$ and $\Lambda = 1$, consists of (2 - $\delta_{0,\Lambda}$) (2 S + 1) = 6 electronic substates $^3\Pi^{e,f}_{\Omega g}$, where (e, f) denotes the parity of the state and $\Omega = |\Lambda + \Sigma|$ with Σ taking (2 S + 1) values from -S to +S. The $\delta_{0,\Lambda}$ is a Kronecker delta (equal to 1 if $\Lambda = 0$ and 0 for all other values).

The method proposed by *Simek and DeBenedictis* [1995] makes use of two main facts: (*i*) the relative populations of the $^3\Pi^{e,f}_{\Omega g}$ substates in the $N_2(B^3\Pi_g)$ electronic state are temperature dependent, and (*ii*) the subband heads formed by individual branches are well separated in wavelengths [*Simek*, 1994].

The method was extended for other 1PG bands [*Simek*, 1994] and, actually, allows using three (v', v'') bands of the N_2 - 1PG corresponding to (2,0), (1,0) and (0,0) transitions, which usually show stronger intensities in the 1PG spectrum, compared to the (3,0) band. The wavelength interval for each of the selected (v', v'') bands is (678 nm - 690 nm) for (3,0), (760 nm - 780 nm) for (2,0), (870 nm - 900 nm) for (1,0) and (1020 nm - 1060 nm) for (0,0).

When applying the method using the (3,0) or (2,0) bands, one needs to take the ratios of the intensities of the second (I_2) and third (I_3) peaks to the intensity of the first sub-band head (I_1) of a given band, that is, one need to experimentally estimate $R_{21} = I_2/I_1 = f_1(\Delta\lambda, T_R)$ and $R_{31} = I_3/I_1 = f_2(\Delta\lambda, T_R)$ in each case. If, instead, one wants to use the (1,0) or (0,0) bands then, in addition to R_{21} and R_{31}, one can also determine $R_{41} = I_4/I_1 = f_3(\Delta\lambda, T_R)$, that is, the ratio of the fourth peak intensity (I_4) to the intensity of the first sub-band head (I_1) of the (1,0) or (0,0) band, respectively. Once R_{21}, R_{31} and R_{41} are known for any of these two bands, *Simek* [1994] provided a procedure to calculate $T_{21} = T_{21}(R_{21}, \Delta\lambda)$, $T_{31} = T_{31}(R_{31}, \Delta\lambda)$ and $T_{41} = T_{41}(R_{41}, \Delta\lambda)$ in a way that, for a given spectral resolution ($\Delta\lambda$), the mean value of T_{21}, T_{31} and T_{41} provides

the rotational (gas) temperature. All the data and coefficients needed to implement this fast T_R estimation method can be found in *Simek and DeBenedictis* [1995] for the (3,0) band and in [*Simek*, 1994] for the (2,0), (1,0) and (0,0) bands. The position of the I_1, I_2, I_3 and I_4 peaks were given by *Simek* [1994] and are now reproduced in Table 1.

The method proposed by *Simek and DeBenedictis* [1995] can be of wide use since the N_2 - 1PG is one of the most accesible band systems of N_2 extending from the red to the near infrared. In addition, since the method deals with optical emissions from the N_2 - 1PG, it can be applied to determine the rotational (gas) temperature in a variety of air plasmas produced in a wide range of pressures from 0.03 mbar ($\simeq$ 75 km altitude) to high pressures (even atmospheric pressure) as long as the the rotational-translation relaxation time at the considered pressure remains much smaller than the characteristic time (τ_q) of the collisional (quenching) deexcitation. Moreover, it allows the calculation of the rotational (gas) temperatures in the range 200 - 1500 K (with a step of dT = 25 K) using medium spectral resolutions that depend on the N_2 - 1PG (v', v'') band selected. In particular, the best sensitivity of the method is achieved when using spectral resolutions in the ranges 0.1 - 0.2 nm for the (3,0) band and 0.2 - 0.3 nm for the (2,0), (1,0) and (0,0) bands. Lower spectral resolutions can be employed, though the sensitivity of the method decreases. The lowest recommended spectral resolutions are, respectively, 0.5 nm, 0.6 nm, 0.68 nm and 0.76 nm for the (3,0), (2,0), (1,0) and (0,0) bands [*Simek*, 1994].

Since 1995, TLE spectroscopy campaigns have provided different spectra of the N_2 - 1PG visible and near infrared optical emissions covering the spectral range between 540 nm and 900 nm. These spectroscopic recordings were done with spectral resolutions of 13 nm (at 900 nm) and 9 nm (at 620 nm) *Morrill et al.* [1998] for 57 km altitude sprite spectrum and 7 nm (across the entire analyzed range of 619 - 897 nm) for 53 km altitude sprite spectrum, 9 nm

(540 - 800 nm) [*Mende et al.*, 1995], 10 nm and 6 nm (540 nm - 840 nm) [*Hampton et al.*, 1996] and 3 nm (640 nm - 820 nm) that is the best resolution so far used [*Kanmae et al.*, 2007]. The papers by *Morrill et al.* [1998] and *Bucsela et al.* [2003] dealt with sprite tendril (53 km and 57 km) spectroscopic observations and provided preliminary spectral data of the N_2 - 1PG (1,0) band up to $\simeq$ 900 nm. However, as acknowledged by the authors, their results regarding 57 km altitude spectra were affected by sensitivity calibration errors, while those of the 53 km altitude spectrum were more certain in the same spectral range *Bucsela et al.* [2003]. These results suggest that the (3,0) and (2,0) bands of the N_2 - 1PG are the most accesible bands to derive the rotational (gas) temperature using the method proposed by *Simek and DeBenedictis* [1995]. However, spectral resolutions one order of magnitude higher than the ones used so far in TLE spectroscopy campagins are needed in order to partially resolve the rotational structure of the different N_2 - 1PG (v', v'') bands selected.

3.1.3. Spectral fitting of $N_2(B^3\Pi_g, v' \rightarrow A^3\Sigma_u^+, v'')$ rovibronic bands

We have developed a program written in python programming language to calculate the synthetic spectrum of the rovibronic bands for the N_2 - 1PG that involves transitions between the upper electronic state $N_2(B^3\Pi_g)$ (with Λ' = 1) and the lower electronic state $N_2(A^3\Sigma_u^+)$ (with Λ" = 0). The $N_2(A^3\Sigma_u^+)$ state (with spin-orbit constant $A_{v''} = 0$) belongs to the Hund's case (b) . However, the coupling of the $N_2(B^3\Pi_g)$ electronic state is type Hund's case (a) for the lower rotational quantum number J' values and Hund's case (b) for J' values higher than 15 [*Herzberg*, 1950]. Therefore, we have considered the intermediate Hund case coupling for the $N_2(B^3\Pi_g)$ state. In calculating the N_2 - 1PG rovibronic band spectrum, we have taken into account the parity (Λ-type doubling) of the 3 substates ${}^3\Pi_{\Omega g}^{e,f}$ of the upper electronic state $N_2(B^3\Pi_g)$. Thus, the triplet fine structure of the $N_2(B^3\Pi_g \rightarrow A^3\Sigma_u^+)$ rovibronic band spectrum consists of a total

of 27 branches divided into the 3 sub-bands $^3\Pi_{0g}^{e,f} \rightarrow {}^3\Sigma_u^+$, $^3\Pi_{1g}^{e,f} \rightarrow {}^3\Sigma_u^+$ and $^3\Pi_{2g}^{e,f} \rightarrow {}^3\Sigma_u^+$ with 9 branches, each denoted *P*, *Q* and *R* that correspond to ΔJ = *J*' - *J*" = -1, 0, +1, respectively. At medium spectral resolutions (0.1 - 0.5 nm) the small spin splitting causes the overlap of the three subbands producing the appearance of, depending on the (v', v'') considered, 3 or 4 sub-band head peaks whose positions are listed in Table 1 [*Simek and DeBenedictis*, 1995], [*Simek*, 1994]. Given a set of (v', v'') vibrational bands within the N_2 - 1PG, the emission intensity of each of the rovibronic transitions considered between (v', J') and (v'', J'') is given by [*Whiting et al.*, 1980]

$$I_{v'',J_j''}^{v',J_j'}(T_R) = N_{v',J_j'}(T_R) A_{v'',J''}^{v',J'} \frac{hc}{\lambda_j} = C_1 \times N_{v',J_j'}(T_R) B_{v''}^{v'} \frac{\nu_j^4 S_{J_j',J_j''}}{2J+1}, \tag{3}$$

where C_1 is a constant and ν_j, $S_{J_j',J_j''}$, v', J_j' and $N_{v',J_j'}$ are, respectively, the frequency, the Hönl-London (or line strength) factor, the vibrational ($0 \le v' \le 12$) and rotational ($2 \le J_j' \le 39$) quantum numbers, and the population of the corresponding upper rovibronic level, each for the *j*-th rotational line. T_R stands for the rotational temperature and $A_{v'',J''}^{v',J'}$ is the Einstein spontaneous emission probability. In equation (3), we have assumed that

$$A_{v'',J''}^{v',J'} = \frac{A_{v''}^{v'} S_{J_j',J_j''}}{(2-\delta_{0,\Lambda})(2S+1)(2J+1)} = \frac{B_{v''}^{v'} S_{J_j',J_j''}}{\lambda_j^3 (2-\delta_{0,\Lambda})(2S+1)(2J+1)} \tag{4}$$

where $B_{v''}^{v'}$ are the (v', v'') Einstein spontaneous emission probabilities tabulated by *Gilmore et al.* [1992]. The $S_{J_j',J_j''}$ rotational line intensity strength factors, that is, the Hönl-London factors, are normalized as $\sum S_{J_j',J_j''} = (2-\delta_{0,\Lambda'}, \delta_{0,\Lambda''})(2S+1)(2J+1)$ [*Whiting et al.*, 1980] where $\delta_{0,\Lambda'}$ and $\delta_{0,\Lambda''}$ are Kronecker deltas (equal to 1 if $\Lambda' = 0$ or $\Lambda'' = 0$ and 0 for all other values) and (2 S + 1) is the spin multiplicity. The summation in $\sum S_{J_j',J_j''}$ is over all allowed transitions from (or to) the group of $(2-\delta_{0,\Lambda})(2S+1)J$ levels with the same value of J' or J'' and, since the $\sum S_{J_j',J_j''}$ sum rule is symmetrical in J' and J'', explicit use of the primes is omitted. In addition, the factor of 2, which appears in the sum rule for all spin-allowed transitions, except $\Sigma^{\pm} \leftrightarrow \Sigma^{\pm}$,

is present because the summation is over both Λ (parity) substates of non Σ states. Following *Whiting et al.* [1980], in $\Sigma \leftrightarrow \Pi$ and $\Pi \leftrightarrow \Sigma$ transitions, even though only the Π state contains two Λ substates, the factor 2 is present in the sum rule of $S_{J'_j,J''_j}$ regardless of which state is the initial one.

Assuming equilibrium (Boltzmann) distribution within the rotational levels, the concentration of a single rotational level ($\boldsymbol{J'_j}$) in each of the electronic substates $^3\Pi^{e,f}_{\Omega g}$ can be written as [*Simek and DeBenedictis*, 1995]

$$N_{v',J'_j}(T_R) = N_{v'} \frac{\exp(\frac{-hc}{kT_R}A_{v'}\Lambda\Sigma)}{1 + 2\cosh(\frac{hc}{kT_R}A_{v'})} \frac{(2J'_j + 1)\exp(\frac{-hc}{kT_R}F(J'_j))}{Q_R(T_R)}\Phi_{J'_j} \tag{5}$$

where v' is the upper vibrational quantum number, $N_{v'}$ is the concentration of the v'th vibrational level, $Q_R = kT_R/hcB_{v'}$, $F(J'_j)$ is the rotational energy of a given upper J'_j rotational level, and $\Phi_{J'_j}$ is an alternation factor which is a function of the nuclear spin I and takes into account the parity $(e,\ f)$ of the considered rotational level. For homonuclear molecules (like N_2) their values are (I + 1)/(2 I + 1) for symmetric levels and I/(2 I + 1) for asymmetric levels. For N_2, I = 1 and thus $\Phi_{J'_j}$ = 2/3 or 1/3 for symmetric levels (e) and asymmetric levels (f), respectively.

Considering equations (3)-(5) and, given a set of (v', v'') vibrational bands within the N_2 - 1PG, the emission intensity of each of the rovibronic transitions considered between (v', J') and (v'', J'') is given by

$$I^{v',J'_j}_{v'',J''_j}(T_R) = C_2 \times N_{v'} \frac{S_{J'_j,J''_j}}{\lambda^4_j} \frac{1}{T_R}\Phi_{J'_j}\exp(\frac{-hc}{kT_R}F(J'_j)), \tag{6}$$

where C_2 is a constant and the $1/T_R$ dependency comes from the expression of $Q_R(T_R)$. In calculating the line intensities, we computed the Hönl-London factors using the formulae given by *Kovacs* [1969] for triplet transitions in the intermediate regime between Hund's case (a) and case (b).

For the electronic states $N_2(B^3\Pi_g)$ and $N_2(A^3\Sigma_u^+)$, every rotational level $\boldsymbol{N}$ is subdivided in three sub-levels with quantum numbers J corresponding to $J = \boldsymbol{N} - 1$, $J = \boldsymbol{N}$ and $J = \boldsymbol{N} + 1$ corresponding, respectively, to the rotational energies $F_3(J'_j)$, $F_2(J'_j)$ and $F_1(J'_j)$. For the rotational energies of each of the three sub-states of $^3\Pi$ states, we have used the expressions given by *Budo* [1935], valid for any degree of spin uncoupling [*Herzberg*, 1950]. For the three sub-states of the lower $^3\Sigma$ electronic state, we have used the formulae for the rotational energy terms from *Mulliken* [1930]; *Roux et al.* [1990]. In order to calculate $F_3(J'_j)$, $F_2(J'_j)$ and $F_1(J'_j)$ we have considered the spin-orbit ($A_v = 0$ for $N_2(A^3\Sigma_u^+)$) rotational and centrifugal spectroscopic constants of the $N_2(B^3\Pi_g)$ and $N_2(A^3\Sigma_u^+)$ states given by *Roux et al.* [1983]. The electronic energies T'_e and T''_e of, respectively, the $N_2(B^3\Pi_g)$ and $N_2(A^3\Sigma_u^+)$ electronic states, together with the spectroscopic constants (ω_e, $\omega_e x_e$, $\omega_e y_e$ and $\omega_e z_e$), needed to evaluate the vibrational energy terms of the $N_2(B^3\Pi_g)$ and $N_2(A^3\Sigma_u^+)$ electronic states, were taken from *Naghizadeh-Kashani et al.* [2002]. For a given (v', v'') transition within the N_2 - 1PG, the wavelengths of each of the 27 rotational lines involved in a (J', J'') rotational band are $\lambda_{kl}^{J',J''}(cm) = 1/(\nu_{ev}(cm^{-1}) + F'_k(J') - F'_l(J''))$, where $\nu_{ev}(cm^{-1}) = (T'_e - T''_e) + G'(v') - G''(v'')$ with $1 \leq k, l \leq 3$ and $\Delta J = J' - J''$. Given the rotational levels J' and J'', the three possible transitions between the subrotational levels (k, l) of, respectively, (J', J''), correspond to those fulfilling ΔJ = -1 (branch P), 0 (branch Q) and +1 (branch R) selection rules. So, we end up having 3 allowed rotational transitions in each of the 9 pairs (k, l).

In order to compare the synthetic spectra with the observed (measured) spectra, each line of the synthetic spectrum needs to be convolved with an instrument function taking into account the finite spectral resolution of the spectrograph used. To model the instrument spectral broadening, we have used a combination of a Gaussian and a Lorentzian function, that is, a Voight function

as [*Biloiu et al.*, 2007]

$$S_{p,w}(\lambda) = p\frac{\sqrt{4\ln 2}}{\sqrt{\pi}w}\exp\left(-\frac{4\ln 2}{w^2}(\lambda - \lambda_{kl}^{J',J''})^2\right) + \frac{2}{\pi}\frac{(1-p)w}{w^2 + 4(\lambda - \lambda_{kl}^{J',J''})^2} \quad (7)$$

where p and $1 - p$ are the relative magnitudes of the Gaussian and Lorentzian functions contributions, respectively, w is a parameter measuring the spectral resolution as the full width at half maximum (FWHM) of the line considered, and $\lambda_{kl}^{J',J''}$ is the central wavelength or the wavelength corresponding to the calculated (synthetic) rotational lines. We have used Gaussian lines shapes ($p = 1$) in spectral fitting of laboratory measured spectra of particular (v', v'') rovibronic transitions of $N_2(B^3\Pi_g \rightarrow A^3\Sigma_u^+)$ recorded with 0.43 nm spectral resolution to obtain tha rotational (gas) temperature (see Figures 4, 5 and 6b, 6c). However, Voight line shapes ($p = 0.5$) were used in spectral fitting of partial N_2 1PG spectra recorded with 2 nm spectral resolution to derive the VDF of $N_2(B^3\Pi_g)$ (see Fig. 8b, 8c).

3.2. Experimental quantification of vibrational distribution functions

In order to experimentally obtain the VDF of $N_2(B^3\Pi_g)$ from laboratory data, we have fitted synthetic spectra of $\mathbf{N}_2$ 1PG to the experimental spectra recorded using different pressures (0.1 mbar - 2 mbar) at low resolution (2 nm). For such a fit, we have used the rotational (gas) temperature resulting from previous fitting of certain rovibronic bands, like (3,0) and (2,0), at medium (0.45 nm) spectral resolution of laboratory HC discharges spectra.

The resulting VDFs were compared with those recorded for sprites by, respectively, *Bucsela et al.* [2003] at 53 km and *Kanmae et al.* [2007] at 53 km and 74 km. In addition, we will compare present VDF laboratory results with available sprite and halo VDF model predictions [*Gordillo-Vázquez*, 2010; *Luque and Gordillo-Vázquez*, 2011; *Gordillo-Vázquez et al.*, 2011, 2012] where a gas temperature of 220 K is assumed.

4. Results and discussion

As mentioned in the introduction, the employment of the so-called Boltzmann plot method using different bands of the first negative system of $N_2^+(B^2\Sigma_u^+ \rightarrow X^2\Sigma_g^+)$ is justified for altitudes between ≃ 60 km and ≃ 48 km (quenching altitude), that is, for pressures between ≃ 0.23 mbar and ≃ 1.5 mbar. This altitude (pressure) region corresponds to the one where giant blue jets, blue jets and sprite tendrils take place.

We have implemented the Boltzmann plot method measuring the relative intensities of the rotational R - branch (ΔJ = +1) of the vibrational transition (0,0) of the first negative system of N_2^+, that is, $N_2{}^+(B^2\Sigma_u^+, v' = 0, J' \rightarrow X^2\Sigma_g^+, v'' = 0, J'')$, with the band head wavelength at 391.4 nm. Since $B_{v'} = B_e + \alpha_e\ (v' + 0.5)$ and the rotational spectroscopic constants for $N_2{}^+(B^2\Sigma_u^+, v' = 0, J')$ are $B_e = 2.085$ cm^{-1} and $\alpha_e = 0.0212$ cm^{-1}, we find that $B_{v'=0} = 2.074$ cm^{-1} and, since hc/k = 1.438 cm K, the slope -$B_{v'=0}$hc/kT_R of equation (2) becomes -2.984/T_R.

The Boltzmann plot method has been applied to air plasmas produced in DC hollow cathode discharges at 2.0 mbar (≃ 45 km), 1.5 mbar (≃ 48 km), 1.0 mbar (≃ 50 km), 0.23 mbar (≃ 60 km) and 0.11 mbar (≃ 70 km) using the Jobin Yvon spectrometer with the fotomultiplier and the CCD, with the 1800 grooves/mm grating, with spectral resolutions of $\Delta\lambda$ = 0.010 nm (FM), 0.020 nm (CCD) and 0.034 nm (CCD), able to resolve nearly completely the rotational structure of the (0,0) vibrational transition of N_2^+ - 1NG. The standard deviation in the slopes of the Boltzmann plot is less than 10 %, which produces an uncertainty in the obtained T_R of about 3 %. Note that due to the even-odd alternation in the rotational quantum numbers [*Herzberg*, 1950], relative line intensities with odd J'' must be multiplied by 2. The wavelengths and $J'(J'+1) = (J''+1)(J''+2)$ values for the R branch (ΔJ = +1) rotational transitions of the (0,0)

vibrational band of the first negative system of $N_2^+(B^2\Sigma_u^+)$ are shown in Table 2. As commented on formerly, an example of the method is given in Figure 2.

The subband head peak and spectral fitting methods to determine the gas temperature have been also applied to air plasmas produced in DC hollow cathode discharges for pressures between 0.11 mbar ($\simeq$ 70 km) and 2 mbar ($\simeq$ 45 km) using the (3,0) and (2,0) bands with spectral resolutions of 0.25 nm and 0.43 nm (subband head peak method) and 0.43 nm (spectral fitting method). The rotational (gas) temperatures derived with the three methods commented above are shown in Figure 3. The temperatures obtained with the Boltzmann plot and subband head peak methods are shown in Figure 3a while Figure 3b shows a comparison between the gas temperatures obtained with the subband head peak and spectral fitting methods. As shown in Figure 3a, the temperature obtained (using the excited state rotational constant $B_{v'}$) with the ion $N_2^+(B^2\Sigma_u^+)$ is higher than that derived using vibrational transitions within $N_2(B^3\Pi_g \rightarrow A^3\Sigma_u^+)$. The reason of this behavior can be due to the different spatial distribution of the excited neutrals $N_2(B^3\Pi_g)$ and excited ions $N_2^+(B^2\Sigma_u^+)$ in the hollow cathode discharges under investigation. Ions (like electrons) are concentrated (both radially and longitudinally) in the center of the hollow cathode discharge [*de los Arcos et al.*, 1998; *Castillo et al.*, 2005; *Méndez et al.*, 2006] while the excited neutrals $N_2(B^3\Pi_g)$ could also reach a maximum in the center (due to the highest value of the electron density there) but with a less steep gradient than excited ions. Consequently, more excited neutrals $N_2(B^3\Pi_g)$ could be located towards the water refrigerated cathode/anode walls where the gas temperature should be smaller than in the center of the discharge, where most ions $N_2^+(B^2\Sigma_u^+)$ are concentrated. In this regard, Figure 3b shows a comparison of the gas temperatures derived when applying the subband head peak and the spectral fitting methods to the (3,0) and (2,0) vibrational transitions of $N_2(B^3\Pi_g \rightarrow A^3\Sigma_u^+)$ using spectral resolutions of

447 0.43 nm and 0.25 nm. We can see in Figure 3b that both methods based on the excited neutral
448 $N_2(B^3\Pi_g)$ show a good agreement.

449 The spectral fitting of the (3,0) and (2,0) vibrational transitions of $N_2(B^3\Pi_g \rightarrow A^3\Sigma_u^+)$ at
450 different pressures are shown in Figure 4 and Figure 5 for a spectral resolution of 0.43 nm.

451 A comparison between the $N_2(B^3\Pi_g)$ 1PG spectrum recorded by a commercial spectrometer
452 (Jobin Yvon-HORIBA FHR 1000) in the hollow cathode air discharge at 0.23 mbar and the
453 spectrum taken by GRASSP from an air commercial lamp at 0.20 mbar is shown in panel A
454 of Figure 6. Both spectra are represented at the same spectral resolution (0.45 nm). We see
455 in Figure 6 (panel A) that the spectrum recorded by GRASSP reproduces well all the spec-
456 tral features visible in the hollow cathode air discharge spectrum recorded with the commercial
457 spectrograph. The main significant difference between the spectra shown in panel A of Figure 6
458 is due to the fact that the hollow cathode air discharge produces relatively cold plasmas with gas
459 temperature of $\simeq$ 400 K (see Figure 3) while the commercial discharge lamps we use generate
460 a plasma with higher gas temperature that promotes the excitation of higher rotational levels
461 (than in the hollow cathode discharge). The excitation of higher rotational levels within each
462 vibrational level (v') changes the shape of the (v', v'') bands of the commercial lamp spectrum
463 recorded by GRASSP with respect to those of the HC spectrum, producing more intense rota-
464 tional emissions to the left of each band head that are responsible for the higher intensity of the
465 (v', v'') band envelope valleys (see the 660 nm - 690 nm spectral region in panel A of Figure 6).
466 Panels B and C of Figure 6 show the spectral fitting of the (5,3) and (5,2) rovibronic transitions
467 in the air commercial lamp $N_2(B^3\Pi_g)$ 1PG spectrum resulting in gas temperatures of 524 K
468 and 656 K, respectively. The different gas temperatures obtained in the air commercial lamp
469 discharge (at 0.2 mbar or 60 km altitude) and in the hollow cathode glow discharges might be

due to the different power densities in the commercial lamp ($\simeq$ 10 W/cm^3) and in the air hollow cathode discharges (0.05 - 0.35 W/cm^3).

We have represented in Figure 7 the VDF of $N_2(B^3\Pi_g)$ experimentally derived from the N_2 1PG 53 km sprite emission spectra [*Bucsela et al.*, 2003; *Kanmae et al.*, 2007], and 74 km emission spectra [*Kanmae et al.*, 2007], from model calculations for halos and sprites [*Gordillo-Vázquez*, 2010; *Luque and Gordillo-Vázquez*, 2011; *Gordillo-Vázquez et al.*, 2011, 2012] and from the present hollow cathode discharges in air. Panel A of Figure 7 shows the VDF of $N_2(B^3\Pi_g)$ obtained from N_2 1PG sprite emission spectra recorded at low altitude (53 km) or relatively high pressure ($\simeq$ 1 mbar). We can see that the available sprite **VDFs** of $N_2(B^3\Pi_g)$ measured by *Bucsela et al.* [2003] and *Kanmae et al.* [2007] coincide between $v' = 2$ and $v' = 7$ with the VDFs of $N_2(B^3\Pi_g)$ derived from emission spectra of 1 mbar hollow cathode discharge in air and from model predictions. The results for $v' = 1$ by *Bucsela et al.* [2003] at 53 km follows the trend predicted by available sprite kinetic models (assuming T_R = 220 K) at higher (74 km) altitudes [*Gordillo-Vázquez*, 2010; *Luque and Gordillo-Vázquez*, 2011; *Gordillo-Vázquez et al.*, 2011, 2012] though differ from the VDF (v' =1) obtained from emission spectra recorded in hollow cathode discharges at 1 mbar. The latter can be due to the more effective excitation of $N_2(B^3\Pi_g)$ ($v' = 1$) in sprites than in hollow cathode air discharges, as can be seen by looking at the ratio of the (1,0) to (2,1) bands of, respectively, the laboratory hollow cathode (lab HC) discharge (solid line) and of the 53 km altitude sprite spectrum (dashed line) recorded by *Bucsela et al.* [2003], shown in panel A of Figure 8. The intensity of the (1,0) band is almost a factor of two higher than the (2,1) band intensity in the 53 km sprite spectrum (dashed line), while it is 40 % lower in the lab HC spectrum (solid line). In panel B of Figure 7 we see a comparison between the VDF of $N_2(B^3\Pi_g)$ recorded from sprite instrument corrected N_2 1PG

emission spectra at 74 km using $\Delta\lambda$ = 3 nm [*Kanmae et al.*, 2007], from a kinetic model (assuming T_R = 220 K) to predict the VDF of $N_2(B^3\Pi_g)$ in sprites and halos at, respectively, 74 km and 80 km [*Luque and Gordillo-Vázquez*, 2011; *Gordillo-Vázquez et al.*, 2011, 2012] and from the $N_2(B^3\Pi_g)$ 1 PG spectrum of a hollow cathode air discharge generated at 0.11 mbar ($\simeq$ 70 km) recorded with $\Delta\lambda$ = 2 nm. The agreement between the experimentally recorded VDF of sprites at 74 km [*Kanmae et al.*, 2007] and the model predicted VDF of sprites and halos is now more evident while at 0.11 mbar the discrepancy with the VDF (v' =1) obtained from emission spectra recorded in hollow cathode discharges persists. It is worth mentioning that, in order to derive the VDF of $N_2(B^3\Pi_g)$ from experimentally recorded N_2 1PG sprite spectra, both *Bucsela et al.* [2003] at 53 km and *Kanmae et al.* [2007] at 53 km and 74 km fitted their observed sprite spectra assuming a rotational (gas) temperature of T_R = 220 K.

Finally, we also see in Figure 8 (panel A) a comparison of the partial N_2 1PG instrument corrected spectra recorded from a sprite at 53 km altitude taken by *Bucsela et al.* [2003] (dashed line) and by *Kanmae et al.* [2007] (circles), from a hollow cathode discharge in air produced at 1 mbar ($\simeq$ 53 km) (solid line) and transmission corrected spectrum of sprites at 74 km obtained from models (dotted lines) incorporating the plasma vibrational kinetics of TLEs [*Gordillo-Vázquez*, 2010; *Luque and Gordillo-Vázquez*, 2011; *Gordillo-Vázquez et al.*, 2011, 2012]. All spectra shown in panel A of Figure 8 were normalized to the (2,0) transition at 773.2 nm and were recorded or calculated at spectral resolutions of $\Delta\lambda$ = 7 nm (sprite at 53 km, [*Bucsela et al.*, 2003]), $\Delta\lambda$ = 3 nm (sprite at 53 km, [*Kanmae et al.*, 2007]), $\Delta\lambda$ = 2 nm (laboratory hollow cathode discharge) and $\Delta\lambda$ = 3 nm (synthetic spectrum produced by a kinetic model of sprites and halos [*Gordillo-Vázquez et al.*, 2012]). The spectra shown in panels B and C of Figure 8 were normalized to the atomic oxygen multiplet line at 777 nm. The shape of the

different (v', v'') bands in the four spectra shown in Figure 8 (panel A) are not completely the same. For example, a sharp line around 777 nm is clearly visible very close to the right of the (2,0) transition of the laboratory HC spectrum (solid line) but is not present in the field recorded spectra nor in the synthetic sprite spectra. The 777 nm feature and the one at $\simeq$ 844 nm between transitions (4,3) and (3,2) are both associated to strong radiative transitions of atomic oxygen. Moreover, the peaks at $\simeq$ 868 nm and $\simeq$ 878 nm to the left and to the right of, respectively, the (2,1) and (1,0) transitions of the N_2 1 PG, might be also due to atomic nitrogen and oxygen emissions, respectively. Finally, the small peaks at $\simeq$ 811 nm and $\simeq$ 823 nm just before and after the (5,4) transition could also be associated to atomic oxygen emissions.

We see in Figure 8 (panel A) that, in general, the laboratory HC air spectrum, the two sprite spectra recorded at 53 km and the synthetic spectrum of sprites at 74 km agree well between 640 nm and 820 nm. However, beyond 820 nm and up to $\simeq$ 900 nm, we see that while the (2,1) and (1,0) transitions in the 53 km sprite spectrum by *Bucsela et al.* [2003] (dashed line) and the synthetic sprite spectrum at 74 km (dotted line) exhibit similar trends (the (1,0) peak higher than the (2,1) one), though with different quantitative values, they behave differently with respect to the trend of the (2,1) and (1,0) transitions in laboratory HC air spectrum, where both transitions reach more or less the same amplitude. The latter explains why the relative population of $v' = 1$ takes a greater value in the $N_2(B^3\Pi_g)$ VDF of sprites than in those of laboratory HC. Finally, panels B and C of Figure 8 show the spectral fitting of the emission spectra (normalized to the 777 nm oxygen line) from the hollow cathode discharges in air at 0.11 mbar and 1 mbar, respectively. The VDF of $N_2(B^3\Pi_g)$ derived from the N_2 1PG spectrum observed in hollow cathode discharges, shown in Figure 7, were derived from the fits shown in panels B and C of Figure 8 using the previously obtained gas temperature values of 385 K (0.11 mbar) and 356

K (1 mbar). It should be noted that, because of the not yet well understood streamer branching dynamics of sprite streamers moving downward, there are no kinetic models available able to predict sprite streamer optical emissions close to the mesopause ($\simeq$ 53 km).

5. Summary and Conclusions

Spectroscopic diagnosis of low pressure (0.1 - 2 mbar) laboratory air glow discharges produced in, respectively, hollow cathode reactors and commercial lamps were used as benchmarks for rotational (gas) temperature determination in TLEs using three different methods requiring high (0.01 nm) and medium (0.1 - 0.5 nm) spectral resolutions. These methods have been implemented with commercial spectrographs (for the glow discharge) and with a recently developed inhouse instrument called GRAnada Sprite Spectrograph and Polarimeter (GRASSP) (for the commercial discharge lamp) designed for medium resolution (0.45 nm) spectroscopic surveys of TLEs. In particular, the high spectral resolution measurements used the so-called Boltzmann plot method to measure the relative intensities of the rotational R - branch (Δ J = +1) of the vibrational band (0,0) of the first negative system of N_2^+, that is, $N_2{}^+(B^2\Sigma_u^+, v' = 0, J' \rightarrow X^2\Sigma_g^+, v'' = 0, J'')$, with the wavelength band head at 391.4 nm. Because of the characteristic rotation-translation relaxation time of $N_2^+(B^2\Sigma_u^+)$ (compared to its radiative lifetime), the use of $N_2^+(B^2\Sigma_u^+ \rightarrow X^2\Sigma_g^+)$ as "thermometer" should be restricted to TLE temperature probing in altitudes equal or lower than 60 km ($\simeq$ 0.23 mbar) down to 48 km ($\simeq$ 1.5 mbar). The other two methods require medium spectral resolution and are based, on one side, on the analysis of several peaks appearing in low lying vibrational transitions, specifically (3,0), (2,0), (1,0) and (0,0), of the N_2 1PG spectrum and on the numerical fitting of synthetic spectrum to the observed (measured) spectrum of the envelope of selected (v', v'') bands of the N_2 1PG spectrum. Since the rotational distribution of $N_2(B^3\Pi_g)$ is already thermalized at $\simeq$ 75

km altitude, the use of $N_2(B^3\Pi_g)$ results in a good "thermometer" in a wide range of altitudes from $\simeq$ 75 km down to $\simeq$ 53 km where collisional (quenching) deactivation prevails over radiative decay. Therefore, the use of $N_2(B^3\Pi_g \rightarrow A^3\Sigma_u^+)$ rovibronic transitions seems justified and very convenient to accurately determine the rotational (gas) temperature in TLE produced air plasmas.

The values of the rotational (gas) temperatures measured in glow discharges produced in DC hollow cathode reactors are almost the same (410 K - 320 K, depending on the pressure used) when the two methods employing $N_2(B^3\Pi_g)$ as the probing species are used, while higher temperatures (with a maximum difference of 100 K at 2 mbar or 45 km altitude) are found when $N_2^+(B^2\Sigma_u^+)$ is tracked. These differences can be principally caused by the spatial distribution of ionic ($N_2^+(B^2\Sigma_u^+)$) and excited neutral ($N_2(B^3\Pi_g)$) species in the hollow cathode discharge used to perform the spectroscopic diagnosis. On the other hand, the gas temperatures in the air commercial lamp discharges (at 0.2 mbar or 60 km altitude) obtained by GRASSP relies on the spectral fitting of certain (v', v'') transitions of $N_2(B^3\Pi_g \rightarrow A^3\Sigma_u^+)$, and the temperatures measured were higher (up to 656 K) than in glow discharges since the power density in the commercial lamp was higher ($\simeq$ 10 W/cm^3) than in the air hollow cathode discharges (0.05 - 0.35 W/cm^3). In addition, the partial N_2 1PG spectrum recorded by GRASSP in air commercial discharge lamps exhibit the same features (though affected by the effect of the different gas temperatures) as the spectrum obtained with commercial spectrographs in air hollow cathode discharges, which supports the reliability of GRASSP for TLE field spectroscopic recordings. It is worth mentioning that the line-of-sight through TLEs (Sprites, Jets, Elves, Halos) is generally not so long as to cover a broad range of temperatures so the methods described in this work can

be used to extract unique temperatures. This is not always the case with remote sensing of the atmosphere.

We found that the relative populations of the vibrational levels of $N_2(B^3\Pi_g)$ from $v' = 2$ to $v' = 7$ are similar in air plasmas produced in laboratory hollow cathode discharges and TLE (sprite) plasmas at different altitudes (53 km - 74 km). However, although the results for $v' = 1$ by *Bucsela et al.* [2003] at 53 km, follow the trend predicted by available sprite kinetic models at higher (74 km) altitudes [*Gordillo-Vázquez*, 2010; *Luque and Gordillo-Vázquez*, 2011; *Gordillo-Vázquez et al.*, 2011, 2012], **they** differ from the VDF (v' =1) obtained from emission spectra recorded in hollow cathode discharges at 1 mbar ($\simeq$ 53 km). The latter can be due to the more effective excitation of $N_2(B^3\Pi_g)$ ($v' = 1$) in sprites than in hollow cathode air discharges. In fact, previous works in auroras [*Cartwright*, 1978; *Morrill and Benesch*, 1996] show that the $N_2(C^3\Pi_u)$ plays a significant role in populating the lower vibrational levels of $N_2(B^3\Pi_g)$. This can also explain the observed TLE (Sprite and Halos) enhancement (with respect to lab results) in the populations of $v' = 0$ and $v' = 1$ in $N_2(B^3\Pi_g)$ [*Bucsela et al.*, 2003], [*Kanmae et al.*, 2007]. The findings by Cartwright [*Cartwright*, 1978], and Morrill and Benesh [*Morrill and Benesch*, 1996] on the kinetics of $N_2(C^3\Pi_u)$ and its impact on the lower vibrational levels of $N_2(B^3\Pi_g)$ were incorporated into the TLE vibrational kinetic models used in this work [*Gordillo-Vázquez*, 2010; *Luque and Gordillo-Vázquez*, 2011; *Gordillo-Vázquez et al.*, 2011, 2012] .

We have found that hollow cathode DC discharges in air produced at low pressure (0.1 - 2 mbar), where wall effects on the plasma excited species are negligible, can be used as reasonable TLE analogs to explore and quantify some TLE spectroscopic features like key emitting species, N_2 1PG spectra, VDF of $N_2(B^3\Pi_g)$ and rotational (gas) temperature. In addition, the VDF of

$N_2(B^3\Pi_g)$ found in hollow cathode DC discharges are quite similar, except the lowest ($v = 0, 1$) vibrational levels, to those derived from TLE N_2 1PG emission spectra.

To conclude, we have tested several spectroscopic techniques that can be applied to TLEs to quantity the gas temperature. According to our study, the best methods to determine the gas temperature in TLE produced air plasmas are those employing $N_2(B^3\Pi_g)$ as the probing species using medium (0.1 - 0.5 nm) spectral resolution spectrographs able to partially resolve the rovibronic band structure of different (v', v'') transitions of $N_2(B^3\Pi_g \rightarrow A^3\Sigma_u^+)$. Spectroscopic methods that use medium spectral resolution have the additional advantage, as compared with higher resolution ones, that they **enable optical systems with larger apertures resulting in better signal to noise ratios at shorter acquisition times**, of great interest in the study of very brief light emitting phenomena such as TLEs. Finally, we have succesfully tested the capabilities of a recently inhouse developed instrument called GRASSP, with 0.45 nm spectral resolution, that we plan to use for TLE spectroscopic surveys in Europe.

Acknowledgments. We thank T. Kanmae and H. C. Stenbaek-Nielsen for kindly providing their sprite spectrum data in the 640 - 820 nm spectral range of a sprite at 53 - 55 km recorded from Langmuir Laboratory and to V. J. Herrero for useful discussions. This work was supported by the Spanish Ministry of Science and Innovation, MINECO under projects AYA2011-29936-C05-02, CSD2009-00038 and FIS2010-16455 and by the Junta de Andalucia, Proyecto de Excelencia FQM-5965. FCPR acknowledges MINECO for a FPI grant BES-2010-042367. AL acknowledges support by a Ramón y Cajal contract, code RYC-2011-07801. EC acknowledges support by a Juan de la Cierva contract, code JdC-2009-04949.

References

Armstrong, R. A., J. A. Shorter, M. J. Taylor, D. M. Suszcynsky, W. A. Lyons, and L. S. Jeong, Photometric measurements in the SPRITES 1995 and 1996 campaigns of nitrogen second positive (399.8 nm) and first negative (427.8 nm) emissions, *J. Atm. Sol.-Terr. Phys.*, *60*, 787, doi:10.1016/S1364-6826(98)00026-1, 1998.

Armstrong, R. A., D. M. Suszcynsky, W. A. Lyons, and T. E. Nelson, Multi-color photometric measurements of ionization and energies in sprites, *Geophys. Res. Lett.*, *27*, 653, doi:10.1029/1999GL003672, 2000.

Biloiu, C., X. Sun, Z. Harvey, and E. Scime, An alternative method for gas temperature determination in nitrogen plasmas: Fits of the bands of the first positive system ($B^3\Pi_g \rightarrow A^3\Sigma_u$), *J. Appl. Phys.*, *101*, 073,303, 2007.

Bucsela, E., J. Morrill, M. Heavner, C. Siefring, S. Berg, D. Hampton, D. Moudry, E. Wescott, and D. Sentman, $N_2(B^3\Pi_g)$ and $N_2^+(A^2\Pi_u)$ vibrational distributions observed in sprites, *J. Atm. Sol.-Terr. Phys.*, *65*, 583, doi:10.1016/S1364-6826(02)00316-4, 2003.

Budo, A., Über dieTriplett-Bandentermformel für den allgemeinen intermediären Fall und Anwendung derselben auf die $B^3\Pi$-$C^3\Pi$-Terme des N_2-Moleküls, *Z. Phys.*, *96*, 219, 1935.

Cartwright, D. C., Vibrational populations of the excited states of N_2 under auroral conditions, *J. Geophys. Res.,* , *83*, 517, doi:10.1029/JA083iA02p00517, 1978.

Castillo, M., V. J. Herrero, and I. Tanarro, Characterization and modeling of the steady state and transients of modulated hollow cathode discharges of nitric oxide, *Plasma Sources. Sci. Technol.*, *11*, 368–376, 2002.

Castillo, M., V. J. Herrero, I. Méndez, and I. Tanarro, Time resolved diagnostics and kinetic modelling of a modulated hollow cathode discharge of NO_2, *Plasma Sources. Sci. Technol.*,

13, 39–47, 2004a.

Castillo, M., V. J. Herrero, I. Méndez, and I. Tanarro, Spectrometric and kinetic study of a modulated glow air discharge, *Plasma Sources. Sci. Technol.*, *13*, 343–350, 2004b.

Castillo, M., I. Méndez, A. M. Islyaikin, V. J. Herrero, and I. Tanarro, Low-pressure DC air plasmas. Investigation of neutral and ion chemistry, *J. Phys. Chem. A*, *109*, 6255–6263, 2005.

de los Arcos, T., C. Domingo, V. J. Herrero, M. Sanz, A. Schulz, and I. Tanarro, Diagnostic and Kinetic Modeling of a Hollow Cathode N_2O Discharge, *J. Phys. Chem. A*, *102*, 6282–6291, 1998.

Franz, R. C., R. J. Nemzek, and J. R. Winckler, Television Image of a Large Upward Electrical Discharge Above a Thunderstorm System, *Science*, *249*, 48, doi: 10.1126/science.249.4964.48, 1990.

Gilmore, F. R., R. R. Laher, and P. J. Espy, Franck-Condon Factors, r-Centroids, Electronic Transition Moments, and Einstein Coefficients for Many Nitrogen and Oxygen Band Systems, *J. Phys. Chem. Ref. Data*, *21*, 1005, doi:10.1063/1.555910, 1992.

Gordillo-Vázquez, F. J., Air plasma kinetics under the influence of sprites, *J. Phys. D*, *41*(23), 234,016, doi:10.1088/0022-3727/41/23/234016, 2008.

Gordillo-Vázquez, F. J., Vibrational kinetics of air plasmas induced by sprites, *J. Geophys. Res. (Space Phys)*, *115*, A00E25, doi:10.1029/2009JA014688, 2010.

Gordillo-Vázquez, F. J., A. Luque, and M. Simek, Spectrum of sprite halos, *J. Geophys. Res. (Space Phys)*, *116*, A09,319, doi:10.1029/2011JA016652, 2011.

Gordillo-Vázquez, F. J., A. Luque, and M. Simek, Near infrared and ultraviolet spectra of TLEs, *J. Geophys. Res. (Space Phys)*, *117*, A05,329, 2012.

Hampton, D. L., M. J. Heavner, E. M. Wescott, and D. D. Sentman, Optical spectral character-

istics of sprites, *Geophys. Res. Lett.*, *23*, 89, doi:10.1029/95GL03587, 1996.

Herzberg, G., *Molecular Spectra and Molecular Structure I. Spectra of Diatomic Molecules*, Van Nostrand Reinhold Co., New York, USA, 1950.

Hirschfelder, C. C. B. R., K. O., *Molecular theory of gases and liquids*, Wiley, New York, USA, 1954.

Kanmae, T., H. C. Stenbaek-Nielsen, and M. G. McHarg, Altitude resolved sprite spectra with 3 ms temporal resolution, *Geophys. Res. Lett.*, *34*, L07,810, doi:10.1029/2006GL028608, 2007.

Kovacs, I., *Rotational Structure in the Spectra of Diatomic Molecules*, American Elsevier, New York, USA, 1969.

Lavrov, B., M. Osiac, A. Pipa, and J. Ropke, On the spectroscopic detection of neutral species in a low-pressure plasma containing boron and hydrogen, *Plasma Sour. Sci. Technol.*, *12*, 576, 2003.

Levine, I. N., *Physical Chemistry*, Mc Graw Hill, New York, USA, 1978.

Luque, A., and F. J. Gordillo-Vázquez, Modeling and analysis of $N_2(B^3\Pi_g)$ and $N_2(C^3\Pi_u)$ vibrational distributions in sprites, *J. Geophys. Res. (Space Phys)*, *116*, A02,306, doi: 10.1029/2010JA015952, 2011.

McDaniel, E., *Atomic collisions, electron and photon projectiles*, John Wiley - Sons, New York, USA, 1989.

Mende, S. B., R. L. Rairden, G. R. Swenson, and W. A. Lyons, Sprite spectra; N_2 1 PG band identification, *Geophys. Res. Lett.*, *22*, 2633, doi:10.1029/95GL02827, 1995.

Méndez, I., F. J. Gordillo-Vázquez, V. J. Herrero, and I. Tanarro, Atom and ion chemistry in low pressure hydrogen DC plasmas, *J. Phys. Chem. A*, *110*, 6060–6066, 2006.

693 Morrill, J., et al., Electron energy and electric field estimates in sprites derived from ionized and
694 neutral N_2 emissions, *Geophys. Res. Lett.*, *29*(10), 1462, doi:10.1029/2001GL014018, 2002.
695 Morrill, J. S., and W. M. Benesch, Auroral N_2 emissions and the effect of collisional pro-
696 cesses on N_2 triplet state vibrational populations, *J. Geophys. Res.,* , *101*, 261, doi:
697 10.1029/95JA02835, 1996.
698 Morrill, J. S., E. J. Bucsela, V. P. Pasko, S. L. Berg, M. J. Heavner, D. R. Moudry, W. M.
699 Benesch, E. M. Wescott, and D. D. Sentman, Time resolved N_2 triplet state vibrational pop-
700 ulations and emissions associated with red sprites, *J. Atm. Sol.-Terr. Phys.*, *60*, 811, doi:
701 10.1016/S1364-6826(98)00031-5, 1998.
702 Moudry, D. R., H. C. Stenbaek-Nielsen, D. D. Sentman, and E. M. Wescott, Velocities of sprite
703 tendrils, *Geophys. Res. Lett.*, *29*(20), 1992, doi:10.1029/2002GL015682, 2002.
704 Mulliken, R. S., The Interpretation of Band Spectra. Parts I, IIa, IIb, *Reviews of Modern Physics*,
705 *2*(1), 60–115, 1930.
706 Naghizadeh-Kashani, Y. Y., Cressault, and A. Gleizes, Net emission coefficient of air thermal
707 plasmas, *J. Phys. D: Appl. Phys.*, *35*, 2925–2934, 2002.
708 Pasko, V. P., U. S. Inan, and T. F. Bell, Spatial structure of sprites, *Geophys. Res. Lett.*, *25*, 2123,
709 doi:10.1029/98GL01242, 1998.
710 Piper, L. G., State-to-state $N_2(A\ ^3\Sigma_u^+)$ energy pooling reactions. II. The formation and quenching
711 of $N_2(B^3\Pi_g$, v=1-12), *Journal Chemical Physics*, *88*, 6911, doi:10.1063/1.454388, 1988.
712 Piper, L. G., The excitation of $N_2(B^3\Pi_g, v = 1 - 12)$ in the reaction between $N_2(A^3\Sigma_u^+)$ and
713 $N_2(X, v \geq 5)$, *Journal Chemical Physics*, *91*, 864, doi:10.1063/1.457138, 1989.
714 Riousset, J. A., V. P. Pasko, and A. Bourdon, Air heating associated with Transient Luminous
715 Events, *AGU Fall Meeting Abstracts*, pp. A293+, 2009.

Riousset, J. A., V. P. Pasko, and A. Bourdon, Air density dependent model for analysis of air heating associated with streamers, leaders, and transient luminous events, *J. Geophys. Res.*, *115*, A12,321, 2010.

Roux, F., F. Michaud, and J. Verges, High-resolution Fourier spectrometry of $^{14}N_2$ infrared emission spectrum: Extensive analysis of the $B^3\Pi_g$-$A^3\Sigma_u^+$ system, *J. Mol. Spectrosc.*, *97*, 253, doi:10.1016/0022-2852(83)90266-7, 1983.

Roux, F., F. Michaud, and M. Vervloet, Investigation of the rovibrational levels of the $B^3\Pi_g$ state of $^{14}N_2$ molecule above the dissociation limit N(^4S) + N(^4S) by Fourier transform spectrometry, *Can. J. Phys.*, *68*, 1257, 1990.

Simek, M., On the use of the numerical simulation of the first positive system of N_2: III. Numerical Thermometer on (v',0) bands, v' = 0-3, *Research Report IPPCZ - 345*, pp. 1 – 31, 1994.

Simek, M., and S. DeBenedictis, On the use of the numerical simulation of the first positive system of N_2: II. Fast T_{rot} Estimation from the Partially Resolved (3,0) Band, *Plasma Chem. Plasma Proc.*, *15*, 451–463, 1995.

Suszcynsky, D. M., R. Roussel-Dupré, W. A. Lyons, and R. A. Armstrong, Blue-light imagery and photometry of sprites, *J. Atm. Sol.-Terr. Phys.*, *60*, 801, doi:10.1016/S1364-6826(98)00027-3, 1998.

Vallance Jones, A., *Aurora*, D. Reidel Publishing Co., Dordrecht, Holland, 1974.

Wescott, E. M., D. D. Sentman, H. C. Stenbaek-Nielsen, P. Huet, M. J. Heavner, and D. R. Moudry, New evidence for the brightness and ionization of blue starters and blue jets, *J. Geophys. Res., , 106*, 21,549, doi:10.1029/2000JA000429, 2001.

738 Whiting, E. E., A. Schadee, J. B. Tatum, J. T. Hougen, and R. W. Nicholls, Recommended con-
739 ventions for defining transition moments and intensity factors in diatomic molecular spectra,
740 *J. Mol. Spectrosc.*, *80*, 249, doi:10.1016/0022-2852(80)90137-X, 1980.

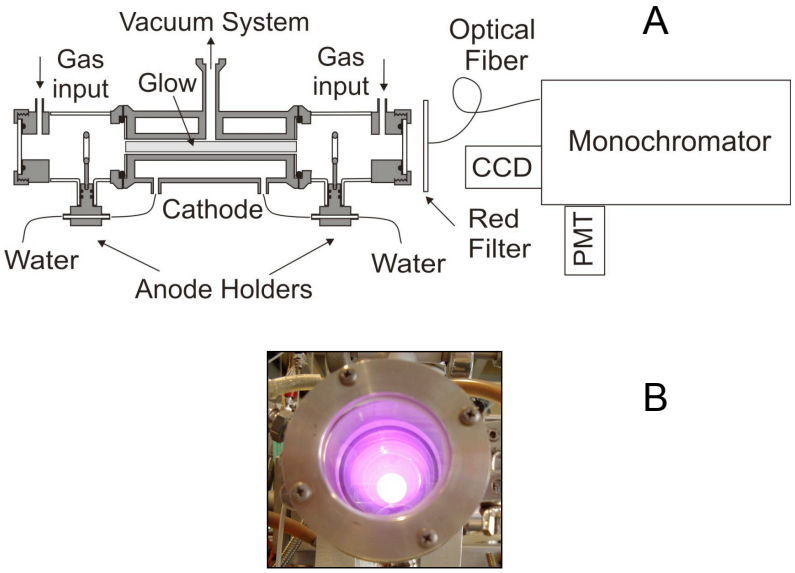

Figure 1. Experimental set up (panel A) of the DC hollow cathode discharge used for spectroscopic diagnosis and an image (panel B) of the generated air plasma where a more intense pink light emission can be seen in the center of the discharge

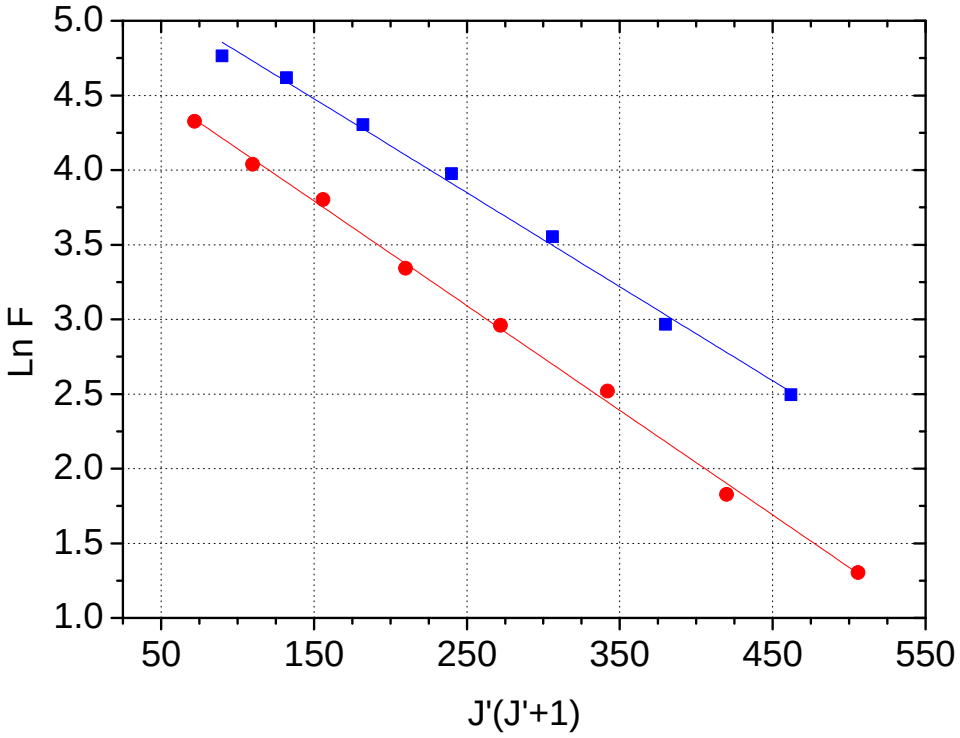

Figure 2. Boltzmann plots ($\ln F$ vs $J'(J'+1) = (J''+1)(J''+2)$, see equation (1)) of the rotational R - branch (ΔJ = +1) transitions involving even (square symbols and blue line) and odd (circles and red line) J'' of $N_2{}^+(B^2\Sigma_u^+, v' = 0, J' \rightarrow X^2\Sigma_g^+, v'' = 0, J'')$ in a 1.5 mbar ($\simeq$ 48 km) DC hollow cathode discharge in air. The rotational (gas) temperatures resulting from the even and odd J'' are 474 K and 426 K, respectively. The $N_2{}^+(B^2\Sigma_u^+, v' = 0, J' \rightarrow X^2\Sigma_g^+, v'' = 0, J'')$ spectrum was recorded with the Jobin-Yvon spectrometer using the CCD and the 1800 grooves/mm grating providing a spectral resolution of 0.023 nm

.

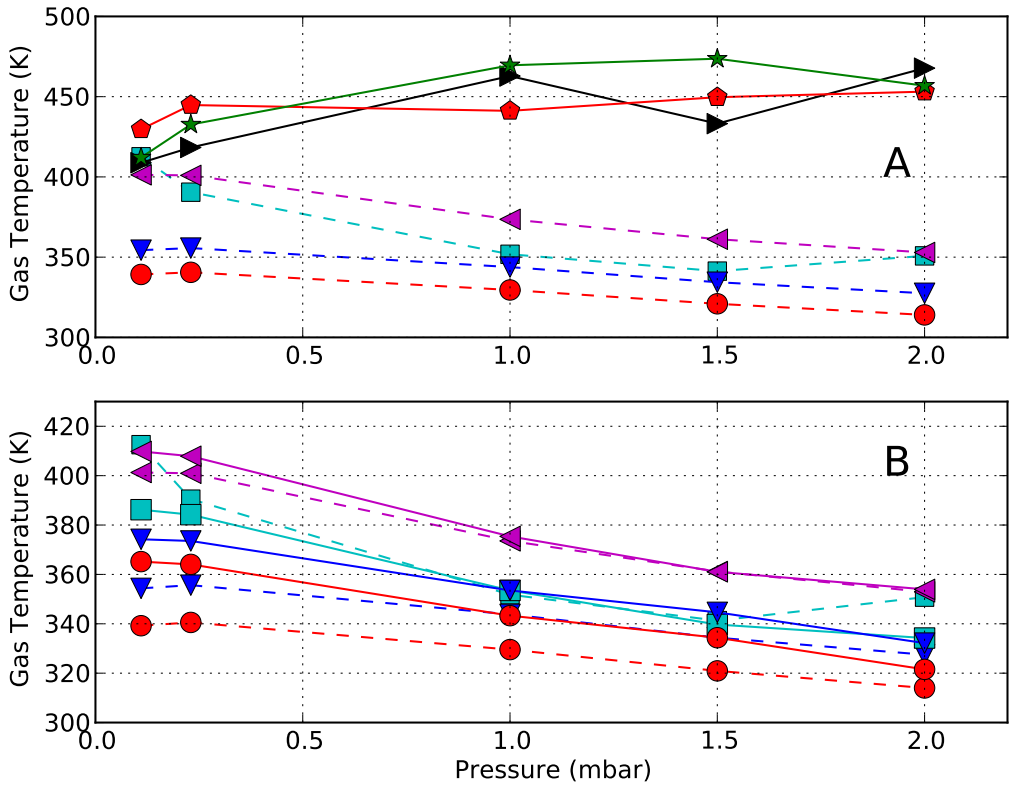

Figure 3. Rotational (gas) temperatures measured in the hollow cathode discharge: (Panel A) derived with the Boltzmann plot of the $N_2^+(B^2\Sigma_u^+)$ (solid line, right triangle FM-0.010 nm; pentagon CCD-0.02 nm; star CCD-0.034 nm) and the sub-band head peak methods applied to the N_2 - 1PG band (dashed line, left triangle (3,0)-0.25 nm; square (3,0)-0.43 nm; down-triangle (2,0)-0.25 nm; circle (2,0)-0.43 nm). (Panel B) derived from the analysis of sub-band head peaks (3,0) and (2,0) recorded (each of them) with two spectral resolutions (0.25 nm and 0.43 nm) (dashed line and symbols correspond to the same data that in panel A) and from spectral fitting methods (solid line, left triangle (3,0)-0.25 nm; square (3,0)-0.43 nm; down-triangle (2,0)-0.25 nm; circle (2,0)-0.43 nm) for different pressures.

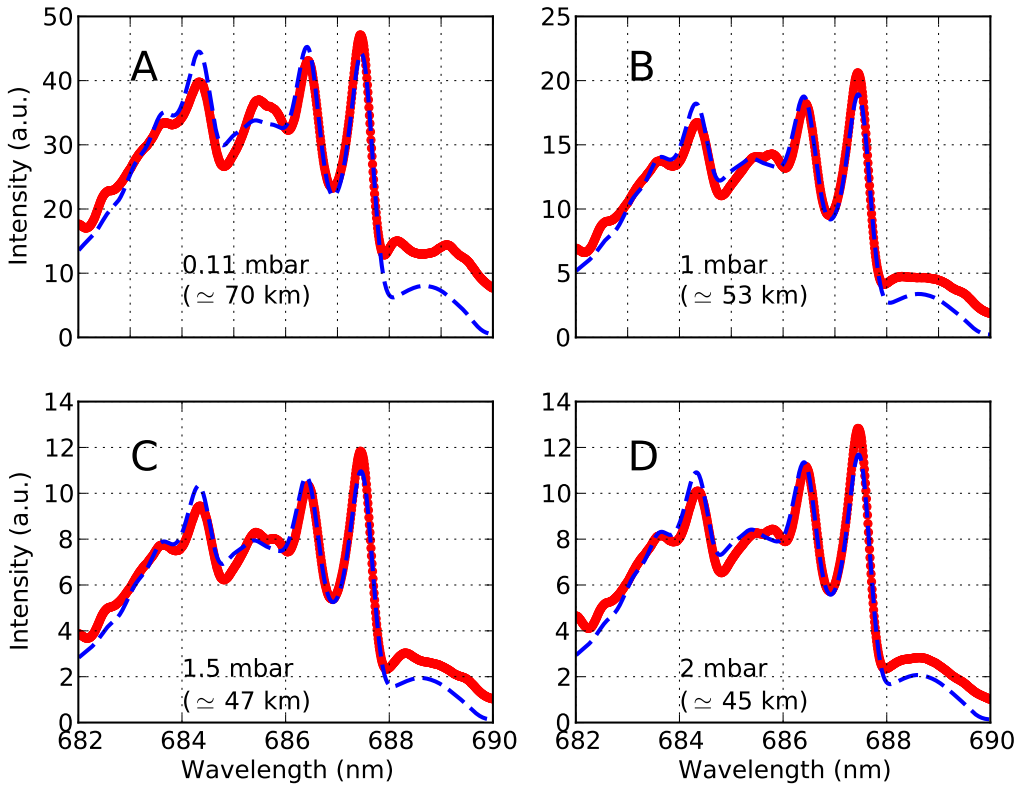

Figure 4. Spectral fitting (dashed blue line) of laboratory measured (solid red line) spectra of the (3,0) rovibronic transitions of $N_2(B^3\Pi_g \rightarrow A^3\Sigma_u^+)$ using 0.43 nm spectral resolution for 0.11 mbar (panel A resulting in T_{gas} = 386 K), 1 mbar (panel B resulting in T_{gas} = 353 K), 1.5 mbar (panel C resulting in T_{gas} = 340 K) and 2 mbar (panel D resulting in T_{gas} = 334 K). The spectra shown in panels A - D were recorded in the laboratory hollow cathode air discharge.

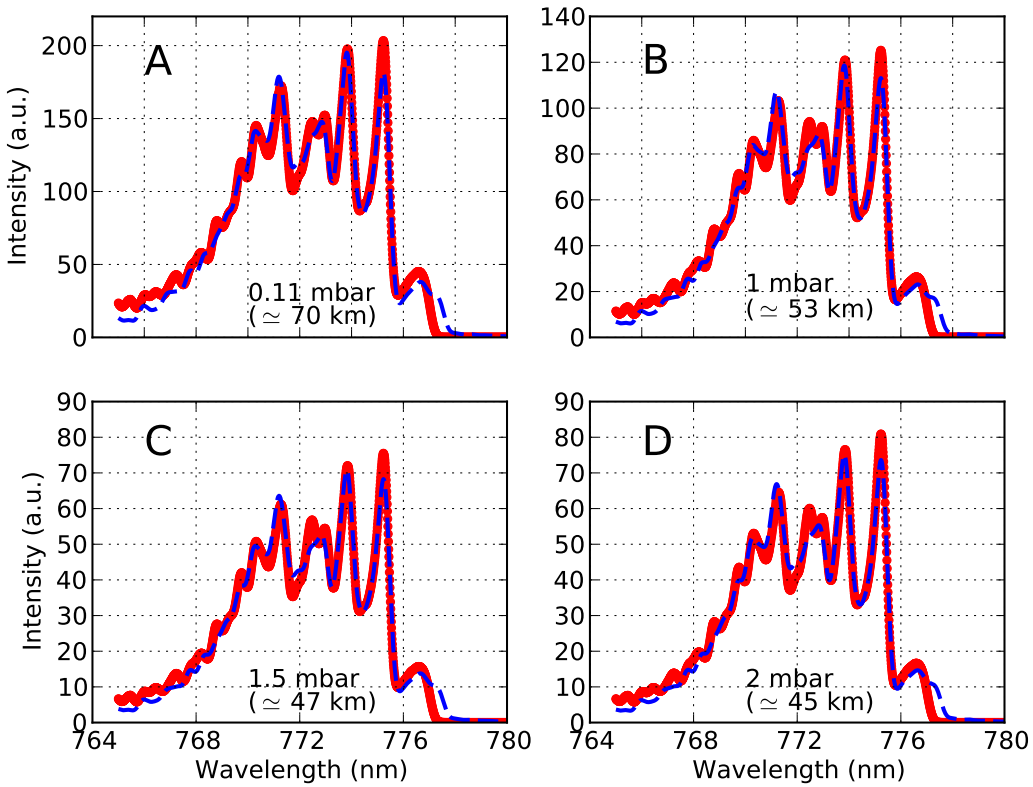

Figure 5. Spectral fitting (dashed blue line) of laboratory measured (solid red line) spectra of the (2,0) rovibronic transitions of $N_2(B^3\Pi_g \rightarrow A^3\Sigma_u^+)$ using 0.43 nm spectral resolution for 0.11 mbar (panel A resulting in T_{gas} = 365 K), 1 mbar (panel B resulting in T_{gas} = 343 K), 1.5 mbar (panel C resulting in T_{gas} = 334 K) and 2 mbar (panel D resulting in T_{gas} = 321 K). The spectra shown in panels A - D were recorded in the laboratory hollow cathode air discharge.

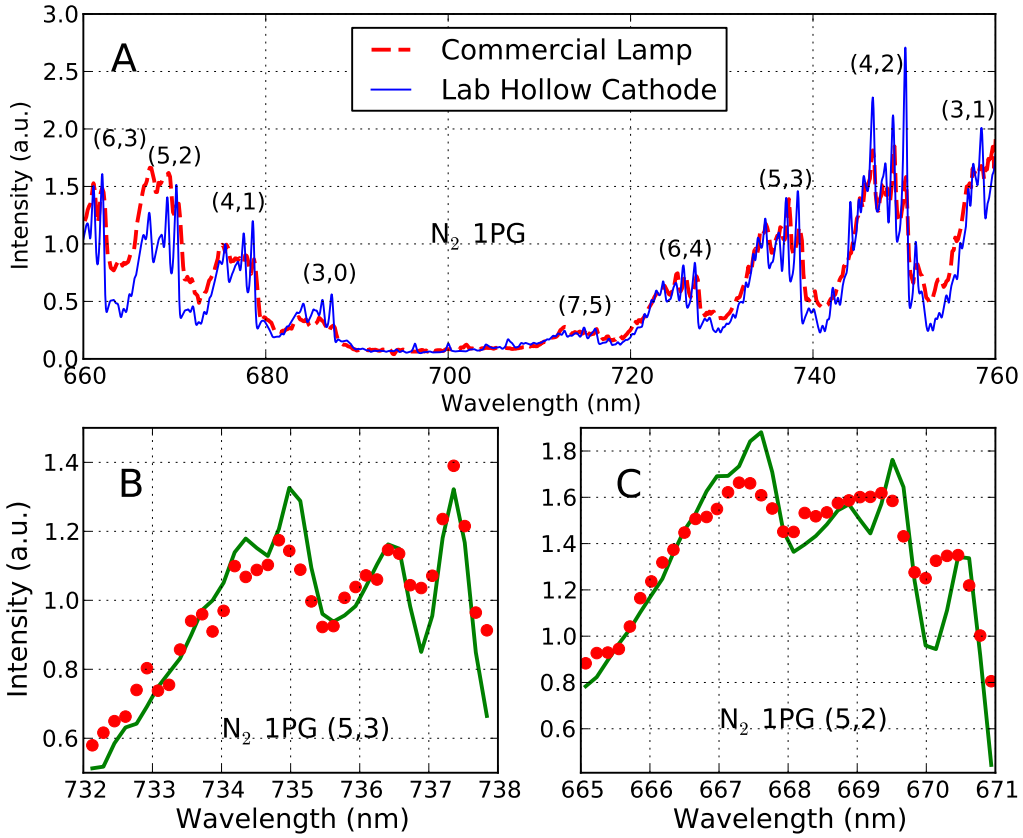

Figure 6. Panel A shows instrument efficiency corrected partial spectra of N_2 1PG band in a hollow cathode air discharge (solid line) at 0.23 mbar recorded by a commercial spectrograph (Jobin Yvon-HORIBA FHR 1000) and of a commerical air discharge lamp (dashed line) at 0.2 mbar taken with GRASSP. Panels B and C show the spectral fitting (solid line) of, respectively, the experimentally recorded (circles) (5,3) and (5,2) rovibronic band transition spectra of N_2 1PG in the commercial air lamp as recorded by GRASSP. The gas temperatures obtained by the (5,3) (panel B) and (5,2) (panel C) fits of the commercial air lamp $\mathbf{N}_2$ 1PG experimental spectrum taken by GRASSP are 524 K and 656 K, respectively. The gas temperature obtained in the hollow cathode discharge at 0.23 mbar is $\simeq$ 380 K (see Figure 3). The spectral resolution used in both cases (hollow cathode and commercial lamp) is 0.43 nm.

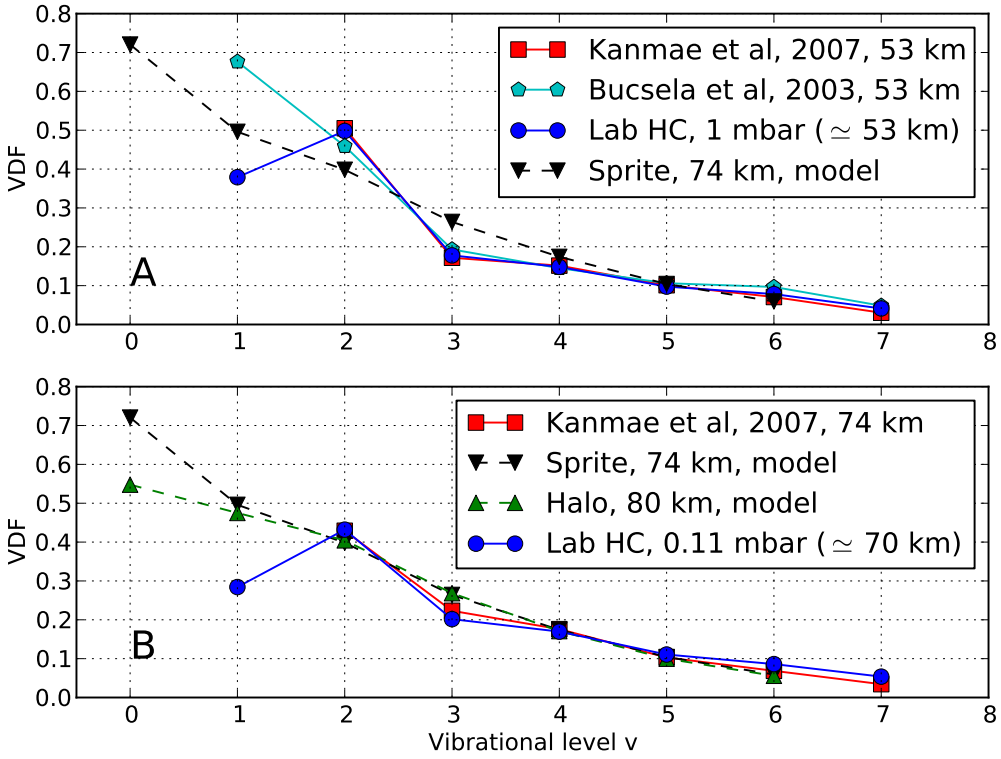

Figure 7. Panel A shows a comparison of the VDF of $N_2(B^3\Pi_g)$ derived from the N_2 1PG instrument corrected sprite emission spectrum at 53 km (≃ 1 mbar) using $\Delta\lambda$ = 7 nm [*Bucsela et al.*, 2003] and $\Delta\lambda$ = 3 nm [*Kanmae et al.*, 2007], from the N_2 1PG spectrum of a hollow cathode air discharge generated at 1 mbar (≃ 53 km) recorded with $\Delta\lambda$ = 2 nm and from a kinetic model to predict the VDF of $N_2(B^3\Pi_g)$ in sprites at 74 km [*Luque and Gordillo-Vázquez*, 2011; *Gordillo-Vázquez et al.*, 2011, 2012]. In panel B we see a comparison between the VDF of $N_2(B^3\Pi_g)$ recorded from the instrument corrected N_2 1PG sprite emission spectra at 74 km using $\Delta\lambda$ = 3 nm [*Kanmae et al.*, 2007], from a kinetic model to predict the VDF of $N_2(B^3\Pi_g)$ in sprites and halos at, respectively, 74 km and 80 km [*Luque and Gordillo-Vázquez*, 2011; *Gordillo-Vázquez et al.*, 2011, 2012] and from the N_2 1PG spectrum of a hollow cathode air discharge generated at 0.11 mbar (≃ 70 km) recorded with $\Delta\lambda$ = 2 nm. The VDF is normalized to the sum of the populations from v' = 2 to v' = 6.

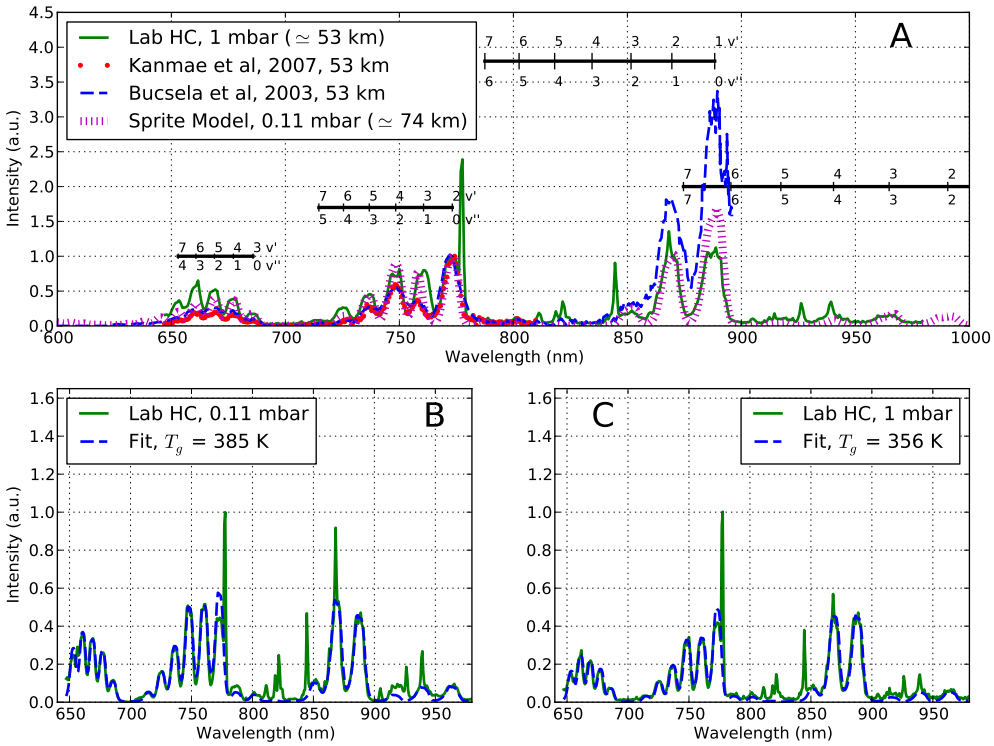

Figure 8. Panel A shows a comparison of the instrument corrected N_2 1PG spectra recorded from sprites at 53 km using $\Delta\lambda$ = 3 nm (circles) [*Kanmae et al.*, 2007] and $\Delta\lambda$ = 7 nm (blue dashed line) [*Bucsela et al.*, 2003], from a laboratory hollow cathode air discharge (green solid line) generated at 1 mbar (≃ 53 km) recorded with $\Delta\lambda$ = 2 nm and a transmission corrected synthetic sprite spectrum (dotted line) for a sprite at 74 km calculated with a kinetic model of sprites and halos assuming $\Delta\lambda$ = 3 nm [*Gordillo-Vázquez et al.*, 2012]. All spectra in panel A are normalized to the (2,0) transition at 773.2 nm while experimental spectra (green solid line) in panels B and C are normalized to the oxygen 777 nm line. Panel B shows the spectral fit (blue dashed line), using T_{gas} = 385 K, to the N_2 1PG spectrum recorded in a hollow cathode air discharge generated at 0.11 mbar (≃ 70 km) recorded with $\Delta\lambda$ = 2 nm. Panel C shows the spectral fit (blue dashed line), using T_{gas} = 356 K, to the N_2 1PG spectrum recorded in a hollow cathode air discharge generated at 1 mbar (≃ 53 km) recorded with $\Delta\lambda$ = 2 nm.

Band	I_1	I_2	I_3	I_4
(0,0)	1050.0 - 1051.2	1047.5 - 1048.5	1045.6 - 1046.4	1053.0 - 1054.5
(1,0)	890.5 - 891.5	888.8 - 889.4	887.5 - 888.1	893.4 - 894.0
(2,0)	774.8 - 775.4	773.5 - 774.1	771.0 - 771.6	-
(3,0)	687.0 - 687.6	686.0 - 686.6	685.2 - 685.8	-

Table 1. I_1, I_2, I_3 and I_4 subband peak positions (nm) of the (0,0), (1,0), (2,0) and (3,0) bands of the N_2 - 1PG

J''	λ (nm)	$(J''+1)(J''+2)$
6	390.49	56
7	390.40	72
8	390.29	90
9	390.19	110
10	390.08	132
11	389.97	156
12	389.85	182
13	389.73	210
14	389.59	240
15	389.43	272
16	389.33	306
17	389.20	342
18	389.04	380
19	388.90	420
20	388.74	462
21	388.58	506

Table 2. Wavelengths and $J'(J'+1) = (J''+1)(J''+2)$ values for the R branch (ΔJ = +1) rotational transitions of the (0,0) vibrational band of the first negative system of $N_2^+(B^2\Sigma_u^+)$